Flow-induced oscillations: A source mechanism for volcanic tremor?

Alison Rust

1 Introduction

Accurate predictions of volcanic activity are key to protecting the hundreds of millions of people who live near potentially active volcanoes. Over the past twenty years, the detection of long-period seismic signals (peak frequencies < 5Hz) has become an increasingly important tool in eruption forecasting, however, the physical mechanisms for their generation remain poorly understood. These long-period ground vibrations that precede and accompany eruptions, may be generated by complex interactions between fluids and rocks. Volcanic eruptions require flow of magma and/or aqueous fluids through rock and there is potential for long-period seismic signals to provide important information on changes in the location, velocity and types of fluids (e.g., gas, magma, bubbly magma) under volcanoes. However, such analysis requires understanding potential source mechanisms of the ground oscillations and the characteristics of the resulting signals. Here we examine the feasibility of inducing persistent long-period seismicity by fluid flow through a crack in an elastic rock, an idea first explored by Julian [1].

2 Characteristics of volcanic tremor

Long-period seismic signals near volcanoes can be of long duration and when a signal continues for several minutes or longer, it is called volcanic tremor. Shorter duration signals with similar waveforms and frequency spectra (and perhaps similar source mechanisms) are simply called long-period (LP) events. Tremor is a common precursor to volcanic eruptions and accompanies nearly all eruptions [2, 3] but the characteristics of tremor can vary considerably. The signal may a) originate from hundreds of meters below the ground surface down to as deep as 40 km, b) have a gradual or abrupt onset, c) be harmonic or anharmonic, and d) last minutes, days or months [2]. Typically, the signal comes from $<$10 km depth, emerges gradually in the time domain with a random distribution of sharp peaks concentrated between 0.1-7 Hz in the frequency domain. There can be systematic changes in tremor during eruptions including period-doubling, a phenomenon associated with a transition from periodic to chaotic behavior of a non-linear system [4, 1].

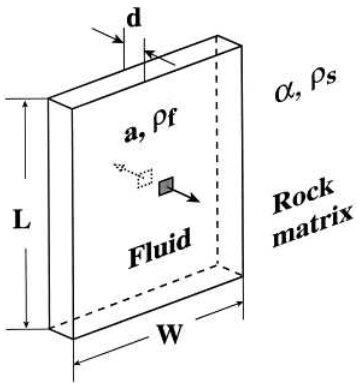

Figure 1: Sketch of the resonating fluid-filled crack model of Chouet [5, 6]. The two small boxes in the center of the crack faces mark where the pressure disturbance that triggers resonance is applied.

3 Models for generation of volcanic tremor

Given the range of tremor properties, depths of origin and association with all styles of eruptions (explosive, effusive; magmatic, phreatic; passive degassing), there are probably multiple origins of volcanic tremor. Several mechanisms for tremor generation have been proposed including bubble growth or collapse, jerky crack propagation, oscillations of magma chambers, resonance of fluid-filled cracks and flow-induced oscillations of conduits. For a review of tremor properties and potential source mechanisms, see [2]. Here we will briefly discuss only two models: 1) the resonance of fluid-filled cracks [5, 6, 7] which is probably the best-known and accepted model for long-period seismicity, and 2) the Julian [1, 4] model of vibrations induced by flow through a slot with elastic walls, which is the inspiration for our analysis.

Chouet [5, 6] proposed that the spectral peaks of tremor and LP events are the resonance modes of fluid-filled cracks. Chouet's model simulates motion along the walls of a rectangular fluid-filled crack in an infinite homogenous elastic solid that is excited into vibrations by a pressure-time source function at a specified position on the walls (Figure 1). The equations of elastic motion of the crack walls are solved simultaneously with the governing equations for fluid flow. The resulting far-field wavefield depends on the crack dimensions, the position and size of the pressure disturbance, the elastic constants of the solid (bulk modulus and rigidity), and the densities and sound speeds of both the solid and fluid. Thus comparing model results to long-period seismic signals recorded at volcanoes, Chouet and others [8, 9] infer parameters such as crack dimensions and sound speeds. There are numerous potential sources of the pressure disturbance required to trigger resonance including an earthquake, a new crack network connection, shock waves from "choked" flow [10], or bubble coalescence leading to a rising gas slug [8]. These are all plausible sources of LP-events, which decay after seconds or tens of seconds. However, tremor requires a disturbance that is sustained for minutes or even months and thus precludes transient resonance triggers such as earthquakes. Sustained resonance could be caused by continued formation of shock waves or gas slugs however these seem to require special circumstances and do not

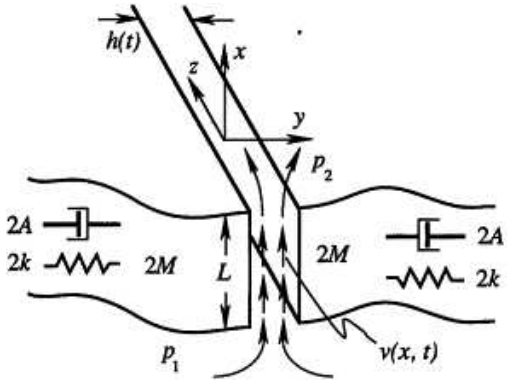

Figure 2: The lumped parameter model of Julian [1] for the generation of tremor by flow induced oscillations. Fluid flows from one reservoir to another (each with constant fluid pressure) via a slot of length L. The walls of the constriction each have a mass M, a stiffness k, and a damping constant A.

explain the near-ubiquity of tremor during volcanic eruptions of all styles and compositions.

If fluid flow through a crack induced oscillations in the conduit walls, this could be a source of sustained seismicity, lasting as long as flow continued at a sufficient speed. Julian [1] explored this tremor mechanism using an approach similar to [11] for blood flow through collapsible arteries. Julian set up a lumped-parameter model involving two-dimensional flow of an incompressible Newtonian fluid through a slot-like constriction with two movable walls (Figure 2). At each end of the constriction the conduit is wide enough that it can be considered to be a fluid reservoir with constant fluid pressure despite oscillations of the constriction. Each wall is modelled as a mass whose motion is controlled by a spring representing the elasticity of the country rock, and a dashpot for anelastic effects and radiation damping. The separation of the walls changes as a function of time only, and thus the walls of the constriction are always flat and parallel. This model leads to a third-order system of nonlinear ordinary differential equations. For different driving fluid pressures, numerical solutions show stable steady flow, simple oscillations, period-doubling cascades, or chaotic oscillations. Although the sample results presented by Julian involve very high fluid velocities (45-110 m/s) and frequencies on the high end of tremor ($\sim$5 Hz), his lumped parameter model demonstrates that flow-induced oscillations are a potential source of tremor and can explain observed non-linear phenomena observed at several volcanoes [4]. Like Julian [1, 4], we consider vibrations induced by fluid flow through an elastic solid. However, we take a mathematically more rigorous approach. Rather than using a lumped parameter model with walls that are blocks with masses connected to springs and dashpots, we assume the conduit is in a homogeneous elastic solid. We solve governing equations for deformation in both the fluid and the solid, and match stresses in the two materials at their interface (the walls). Unlike Julian, we allow the crack gap thickness to vary with both time and position (along the direction of dominant fluid flow). We also consider a tube-like conduit in addition to a slot-like geometry.

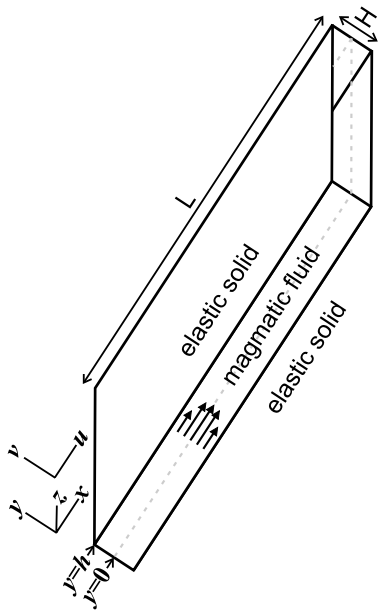

Figure 3: The geometry of our model. An incompressible, Newtonian fluid flows through a crack of length L and equilibrium gap thickness H in an elastic solid. Flow-induced oscillations cause the thickness of the gap ($2h$) to vary in both x and time. Flow is two-dimensional with flow field $(u, v, 0)$ and $u \gg v$.

4 The fluid

We consider flow of an incompressible, Newtonian fluid through a crack of length L and gap thickness H in an isotropic elastic solid (Figure 3). The coordinate system (x, y, z) is set so that the crack is parallel to $y = 0$ and the two crack walls are at $y = \pm h(x, t)$ with $h = \frac{H}{2}$ at equilibrium. Flow is two-dimensional with velocity field $(u, v, 0)$. The governing equations for fluid flow are conservation of momentum,

$$u_t + uu_x + vu_y = -\frac{P_x}{\rho} + \nu(u_{xx} + u_{yy}), \tag{1}$$

and

$$u_t + uv_x + vv_y = -\frac{P_y}{\rho} + \nu(u_{xx} + u_{yy}), \tag{2}$$

and continuity (conservation of mass),

$$u_x + v_y = 0, \tag{3}$$

where ρ is the density, P is the pressure and ν is the kinematic viscosity of the fluid. To simplify this set of equations, we will take advantage of the small aspect ratio, $\epsilon = \frac{H}{L}$, of the fluid-filled crack. We begin by non-dimensionalizing the equations, using

$$x = L\tilde{x}, \quad y = H\tilde{y}, \quad u = U\tilde{u}, \quad v = \epsilon U\tilde{v}, \quad t = \frac{L}{U}\tilde{t} \text{ and } P = [P]\tilde{P}, \tag{4}$$

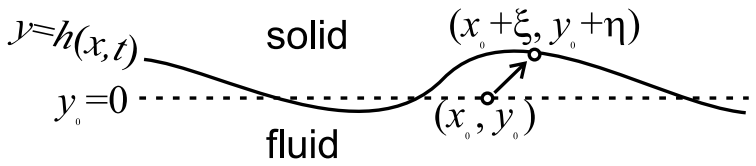

Figure 4: Sketch of the wall for which $h > 0$ at equilibrium. A point in the elastic solid with coordinates (x_0, y_0) at equilibrium has coordinates $(x_0 + \xi,\ y_0 + \eta)$ when disturbed by flow-induced oscillations. The dashed line is the equilibrium position of the fluid-rock interface; $y_0 = 0$ for all points on this line. When deformed this interface becomes the curve $h(x, t)$.

where $\tilde{}$ indicates a dimensionless variable, U is the average fluid speed and $[P] = \frac{U\nu\rho L}{H^2}$. The resulting dimensionless momentum equations to order ϵ^2 are

$$\epsilon\, Re\,(\tilde{u}_{\tilde{t}} + \tilde{u}\tilde{u}_{\tilde{x}} + \tilde{v}\tilde{u}_{\tilde{y}}) = -\tilde{P}_{\tilde{x}} + \tilde{u}_{\tilde{y}\tilde{y}}, \quad \tilde{P}_{\tilde{y}} = 0, \tag{5}$$

where $Re = \frac{UH}{\nu}$ is a Reynolds number using the crack gap thickness for the length-scale. Dropping the $\tilde{}$ notation, the dimensionless equations for momentum are

$$\epsilon\, Re\,(u_t + uu_x + vu_y) = -P_x + u_{yy}, \quad P_y = 0. \tag{6}$$

The base state is $P_x = u_{yy}$. Therefore at equilibrium (i.e., no flow-induced movement of the walls), the non-dimensional pressure gradient and pressure are $P_x = -3$ and $P = -3x$, respectively. The equilibrium fluid thickness, H, is the wall separation caused by the equilibrium fluid pressure. The pressure gradient driving flow will in fact cause the base state to be a wedge-shaped crack. However, we assume H is independent of x, which is a good assumption if the ambient (lithostatic) pressure is much greater than both the fluid pressure and changes in lithostatic pressure along the crack.

The fluid stress tensor is

$$\sigma_{fluid} = \begin{pmatrix} -P & 0 \\ 0 & -P \end{pmatrix} + \nu\rho \begin{pmatrix} 2u_x & u_y + v_x \\ u_y + v_x & 2v_y \end{pmatrix}. \tag{7}$$

Using the continuity equation (3) and the scalings in (4), the non-dimensional fluid stress is, to order ϵ^2,

$$\sigma_{fluid} = [P] \begin{pmatrix} -P & \epsilon u_y \\ \epsilon u_y & -P \end{pmatrix}. \tag{8}$$

5 The solid

We treat the country rock as an elastic solid. The coordinates of a point in the solid are $(x_0 + \xi, y_0 + \eta)$, where (x_0, y_0) is the undisturbed position and $y_0 = 0$ at the wall. To determine non-dimensional governing equations, we assume the wall moves a distance of order $\epsilon L = H$ and take H to be the unit of ξ and η, but L for x_0 and y_0:

$$x_0 = L\tilde{x}_0, \quad y_0 = L\tilde{y}_0, \quad \xi = H\tilde{\xi}, \quad \eta = H\tilde{\eta}. \tag{9}$$

Then, at the wall we have the non-dimensional relations

$$x = x_0 + \epsilon\, \xi_t(x_0, 0, t), \tag{10}$$
$$v(x, h, t) = \eta_t(x_0, 0, t), \tag{11}$$
$$u(x, h, t) = \epsilon\, \xi_t(x_0, t), \tag{12}$$

and taking the non-dimensional location of the wall, $h(x,t)$, to be $h_0 = 1$ when not disturbed,

$$\eta(x_0, 0, t) = h(x, t) - 1. \tag{13}$$

The constitutive equations for stress in the elastic solid are

$$\sigma_{xx} = \lambda(\xi_x + \eta_y) + 2\mu\, \xi_x, \tag{14}$$
$$\sigma_{yy} = \lambda(\xi_x + \eta_y) + 2\mu\, \eta_x, \text{ and} \tag{15}$$
$$\sigma_{xy} = \mu(\xi_y + \eta_x). \tag{16}$$

Again omitting the ˜ notation, the non-dimensional stress tensor for the solid to order ϵ^2 is

$$\sigma_{solid} = \mu\epsilon \begin{pmatrix} 2\xi_{x_0} + \frac{\lambda}{\mu}(\xi_{x_0} + \eta_{y_0}) & \xi_{y_0} + \eta_{x_0} \\ \xi_{y_0} + \eta_{x_0} & 2\eta_{x_0} + \frac{\lambda}{\mu}(\xi_{x_0} + \eta_{y_0}) \end{pmatrix}. \tag{17}$$

We are interested in seismic waves created by oscillations of the crack. We express the elastic wave equations in terms of potentials, ϕ and ψ which are related to ξ and η by

$$\xi = \phi_{x_0} + \psi_{y_0} \text{ and } \eta = \phi_{y_0} + \psi_{x_0}. \tag{18}$$

The wave equations are

$$\phi_{tt} = \alpha^2 \nabla^2 \phi \text{ and } \psi_{tt} = \alpha^2 \nabla^2 \psi, \tag{19}$$

where α and β are compression and shear waves velocities, respectively. Using the average fluid speed to non-dimensionalize the elastic wave speeds,

$$\tilde{\alpha}^2 = \frac{\lambda + 2\mu}{\rho\, U^2} \text{ and } \tilde{\beta}^2 = \frac{\mu}{\rho\, U^2}, \tag{20}$$

where λ and μ are Lame elastic constants (μ is called the shear modulus).

Fourier transform solutions to the wave equations are

$$\phi = \int_{\omega=-\infty}^{\infty} \int_{k=-\infty}^{\infty} e^{ikx_0 + i\omega t}\, \Phi(k, \omega) \frac{dk\, d\omega}{2\pi}\ e^{-\kappa_\alpha\, y_0}, \tag{21}$$

and

$$\psi = \int_{\omega=-\infty}^{\infty} \int_{k=-\infty}^{\infty} e^{ikx_0 + i\omega t}\, \Psi(k, \omega) \frac{dk\, d\omega}{2\pi}\ e^{-\kappa_\beta\, y_0}, \tag{22}$$

where

$$\kappa_\alpha = \sqrt{k^2 - \frac{\omega^2}{\alpha^2}} \text{ and } \kappa_\beta = \sqrt{k^2 - \frac{\omega^2}{\beta^2}}. \tag{23}$$

To ensure that the waves are evanescent (decay as go to an infinite distance from the source), we require that κ_α and κ_β be positive.

6 Matching fluid and solid stresses at the wall

Stress must be continuous across the fluid-solid interface. Therefore from (7) and (17), at $x = x_0 + \mathcal{O}(\epsilon)$ and $y_0 = 0$ (i.e., at the wall),

$$G \begin{pmatrix} 2\xi_{x_0} + \frac{\lambda}{\mu}(\xi_{x_0} + \eta_{y_0}) & \xi_{y_0} + \eta_{x_0} \\ \xi_{y_0} + \eta_{x_0} & 2\eta_{x_0} + \frac{\lambda}{\mu}(\xi_{x_0} + \eta_{y_0}) \end{pmatrix} \begin{pmatrix} -\epsilon h_x \\ 1 \end{pmatrix} = \begin{pmatrix} -P & \epsilon u_y \\ \epsilon u_y & -P \end{pmatrix} \begin{pmatrix} -\epsilon h_x \\ 1 \end{pmatrix}, \tag{24}$$

where

$$G = \frac{\mu\epsilon}{[P]} = \frac{\epsilon^3 \beta^2 L}{U\nu}, \tag{25}$$

and $(-\epsilon h_x, 1)$ is a vector normal to the wall. This gives

$$\xi_{y_0} + \eta_{x_0} = \mathcal{O}(\epsilon) \text{ and } G\left(2\,\xi_{y_0} + \frac{\lambda}{\mu}(\xi_x + \eta_y)\right) = -P + \mathcal{O}(\epsilon), \tag{26}$$

indicating that normal stresses dominate over shear stresses on the wall. Thus the full matching conditions at the wall are

$$x = x_0, \tag{27}$$

$$\xi = h - 1, \tag{28}$$

$$u = 0, \text{ and} \tag{29}$$

$$P = -G\left(2\,\xi_{y_0} + \frac{\lambda}{\mu}(\xi_x + \eta_y)\right). \tag{30}$$

From these conditions and equations (18, 19), for wave-like disturbances,

$$P = G[h(x,t) - 1]\beta^2 \left(\frac{\kappa_\beta^2 + k^2}{\omega^2 \kappa_\alpha}\right)\left(\frac{\omega^2}{\beta^2} - 2k^2 + \frac{4k^2\kappa_\alpha\kappa_\beta}{\kappa_\beta^2 + k^2}\right). \tag{31}$$

For nonlinear stability analysis we calculate an equivalent Fourier Transform solution,

$$\begin{aligned} P =& G\int_{\omega=-\infty}^{\infty}\int_{k=-\infty}^{\infty} e^{ikx+i\omega t}\beta^2 \left(\frac{\kappa_\beta^2 + k^2}{\omega^2\kappa_\alpha}\right)\left(\frac{\omega^2}{\beta^2} - 2k^2 + \frac{4k^2\kappa_\alpha\kappa_\beta}{\kappa_\beta^2 + k^2}\right) \ldots \\ &\ldots \int_{x'=-\infty}^{\infty}\int_{t'=-\infty}^{\infty} e^{-(ikx'+i\omega t')}[h(x',t') - 1]\frac{dt'\,dx'}{2\pi}\frac{dk\,d\omega}{2\pi}, \end{aligned} \tag{32}$$

which for $\omega << \alpha$ and $\omega << \beta$ simplifies to

$$P = 2G\left(\frac{\alpha^2 - \beta^2}{\alpha^2}\right)\int_{x'=-\infty}^{\infty}[h(x',t) - 1]\int_{k=-\infty}^{\infty} \mid k \mid e^{ik(x-x')}\,\frac{dk\,dx'}{2\pi}. \tag{33}$$

7 Linear stability analysis

7.1 Lubrication theory

We begin by considering the case where the crack gap is so thin compared to its length, and flow is slow enough that $\epsilon Re \to 0$. Thus

$$P_x = u_{yy}, \tag{34}$$

which for a parabolic velocity profile and $u = 0$ at the walls gives

$$u = \frac{1}{2} P_x (y^2 - h^2). \tag{35}$$

We next integrate the continuity equation (3) in y and apply a kinematic boundary condition,

$$h_t = v, \tag{36}$$

to obtain

$$h_t - \frac{1}{3} \frac{\partial}{\partial x} h^3 P_x = 0. \tag{37}$$

Adding small perturbations in crack thickness and pressure

$$h = 1 + h' e^{ikx + i\omega t} \text{ and} \tag{38}$$

$$P = -3x + P' e^{ikx + i\omega t}, \tag{39}$$

we solve (37) using P' determined from (31). The resulting linearized dispersion relation is

$$i\omega + 3ik + \frac{1}{3} k^2 \beta^2 G \left(\frac{k^2 + \kappa_\beta^2}{\kappa_\alpha \omega^2} \right) \left(\frac{\omega^2}{\beta^2} - 2k^2 + \frac{4k^2 \kappa_\alpha \kappa_\beta}{k^2 + \kappa_\beta^2} \right) = 0. \tag{40}$$

The system will be unstable if there is a root for which the imaginary part of ω is negative ($\mathcal{I}(\omega) < 0$). This is because $i\omega = i\mathcal{R}(\omega) - \mathcal{I}(\omega)$ and so if $\mathcal{I}(\omega) < 0$ then $e^{ikx + i\omega t}$ will grow with time. For small k, roots are of the form $\omega = -3k + \mathcal{O}(k^3)$. If $\omega = -3k + \omega_{(3)} k^3$, then

$$i\omega_{(3)} \approx \frac{G\beta^2}{27\sqrt{1 - \frac{9}{\alpha^2}}} \left[\left(2 - \frac{9}{\beta^2} \right)^2 - 4\sqrt{\left(1 - \frac{9}{\alpha^2} \right) \left(1 - \frac{9}{\beta^2} \right)} \right]. \tag{41}$$

It is always true that $\beta \leq \alpha$ (20). It is reasonable to assume that $\beta > 3$, which means that the shear wave speed in the country rock (of order km/s) is more than triple the average fluid speed in the crack. With these constraints, we find $i\omega_{(3)} \geq \frac{3G}{\beta^2 \sqrt{1 - \frac{9}{\alpha^2}}}$ and $i\omega_{(3)} > 0$. Therefore, the imaginary part of ω is positive and instabilities will not grow with time.

For large k, roots of equation (40) satisfy

$$\left(1 - \frac{X}{2} \right)^2 - \sqrt{\left(1 - \frac{\beta^2}{\alpha^2} X \right) (1 - X)} = 0, \quad \text{where } X = \frac{\omega^2}{\beta^2 k^2}.$$

There are roots with $\mathcal{I}(\omega) < 0$ but none satisfy $\kappa_\alpha > 0$ and $\kappa_\beta > 0$ as required for evanescence. There are Rayleigh waves propagating along the surface, though, with small $\mathcal{I}(\omega) \geq 0$, that become damped due to fluid viscosity.

7.2 Averaged model

To allow Reynolds number (Re) dependence, while still taking advantage of the small crack gap to length ratio, we average the velocity across the gap (i.e., in the y-direction). We assume the fluid velocity in the crack is

$$u = \frac{3}{2}U\left(1 - \frac{y^2}{h^2}\right) \tag{42}$$

and thus has a parabolic profile with $u = 0$ at the wall ($y = h$), and an average velocity of U.

The momentum equation (6) averaged over y is

$$\epsilon\, Re \int_{y=0}^{h} u_t + uu_x + vu_y\, dy \; = -h\, P_x + [u_y]_{y=h}, \tag{43}$$

which, for u defined in (42), is

$$\epsilon Re\left[\frac{\partial}{\partial t}(Uh) + \frac{\partial}{\partial x}\left(\frac{6}{5}U^2 h\right)\right] = -h\, P_x - \frac{3U}{h}. \tag{44}$$

Similarly the kinematic boundary condition (36) averaged over y is

$$h_t + \frac{\partial}{\partial x}\int_{y=0}^{h} u\, dy = 0, \tag{45}$$

which gives

$$h_t + U_x h + U h_x = 0. \tag{46}$$

Combining (38, 39, 44, 46) and

$$U = 1 + U' e^{ikx + i\omega t}, \tag{47}$$

gives the dispersion relation

$$i\epsilon Re\left(\frac{\omega^2}{k} + \frac{12}{5}\omega + \frac{6}{5}k\right) + 9 + \frac{3\omega}{k} - ikG\beta^2\left(\frac{\kappa_\beta^2 + k^2}{\omega^2\kappa_\alpha}\right)\left(\frac{\omega^2}{\beta^2} - 2k^2 + \frac{4k^2\kappa_\alpha\kappa_\beta}{\kappa_\beta^2 + k^2}\right) = 0, \tag{48}$$

which at $Re = 0$, reduces to the stable result from lubrication theory (40).

From asymptotic analysis for small k, roots of (48) at neutral stability are of the form

$$\omega = -3k + \omega_{(3)}k^3 \tag{49}$$

where

$$\omega_{(3)} = -i\frac{\epsilon Re}{k} + i\frac{G\beta^2}{27\, f_\alpha}\left(1 + f_\beta^2\right)\left(\frac{9}{\beta^2} - 2 + \frac{4f_\alpha f_\beta}{1 + f_\beta^2}\right), \tag{50}$$

and

$$f_\alpha = \sqrt{1 - \frac{9}{\alpha^2}} \text{ and } f_\beta = \sqrt{1 - \frac{9}{\beta^2}}. \tag{51}$$

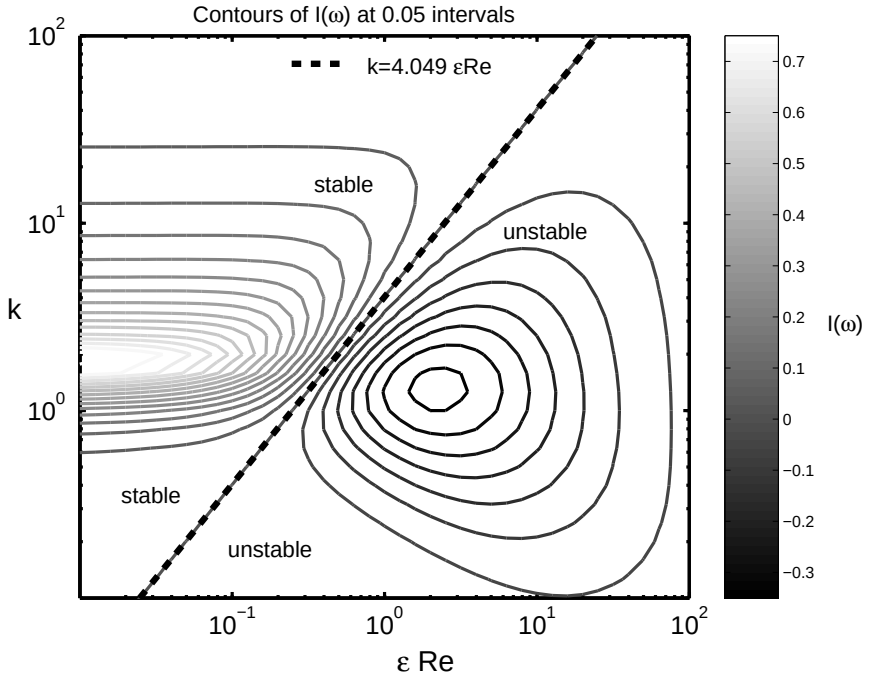

Figure 5: Contours of the imaginary part of the frequency at intervals of 0.05 in a non-dimensional wavenumber versus ϵRe plot. The non-dimensional α and β are set at 8 and 4, respectively. The thick dashed line is the calculated solution (equation 52) for neutral stability of the system. As expected, this line coincides with the $\mathcal{I}(\omega) = 0$ contour. For the parameters used to create this plot, the system is most unstable (fastest growth rate of waves) at both k and ϵRe $\mathcal{O}(1)$. Equivalent plots with α and β one or two orders of magnitude greater show similar patterns with the line of neutral stability matching equation (52).

Hence the waves are unstable if Re is large enough. At neutral stability, $\mathcal{I}(\omega) = 0$, which in this case means $\mathcal{I}(\omega_{(3)}) = 0$. Therefore the non-dimensional critical wave number, $\tilde{k}_{cr}$ (for clarity we return to the ˜ notation to denote non-dimensional quantities), below which the system is unstable is

$$\tilde{k}_{cr} = \frac{27\epsilon Re f_{\tilde{\alpha}}}{G\tilde{\beta}^2\left(1+f_{\tilde{\beta}}^2\right)\left(\frac{9}{\tilde{\beta}^2}-2+\frac{4f_{\tilde{\alpha}}f_{\tilde{\beta}}}{1+f_{\tilde{\beta}}^2}\right)}, \tag{52}$$

which is equivalent to

$$\tilde{k}_{cr} = \left(\frac{27\,U^4}{\epsilon\ \beta^4}\right)\frac{f_{\tilde{\alpha}}}{\left(1+f_{\tilde{\beta}}^2\right)\left(\frac{9}{\tilde{\beta}^2}-2+\frac{4f_{\tilde{\alpha}}f_{\tilde{\beta}}}{1+f_{\tilde{\beta}}^2}\right)}, \tag{53}$$

where β without the ˜ is the true dimensional shear wave speed. Note that $\tilde{k}_{cr} = 1$ corresponds to a wave of wavelength equal to the length of the crack and the second fraction in (53) is of order 1. Interestingly, $\tilde{k}_{cr}$ is proportional to the reciprocal of a Mach number to the fourth power and does not directly depend on the fluid viscosity. Furthermore, from (53) the system could be unstable at arbitrarily low ϵRe.

7.3 Long wave expansion

Typically, results from an averaged model are qualitatively correct with some error from the averaging. To check the accuracy of the averaging results at small k we use asymptotic analysis. We begin by defining stream functions that satisfy continuity

$$u = \chi_y + U(y),\ \ v = -\chi_x, \tag{54}$$

where $\chi \propto e^{ikx+i\omega t}$. In terms of these stream functions, the momentum equation in x is

$$\epsilon Re\left(i\omega\chi_y + \frac{3}{2}\left(1-y^2\right)ik\chi_y + 3ik\chi_y\right) = -ik\hat{p} + \chi_{yyy}. \tag{55}$$

Solving for ω to order ϵ^2 using

$$\epsilon Re = \sum_{n=0}^{\infty} R_{(n)}k^n,\ \ \omega = \sum_{n=1}^{\infty}\omega_{(n)}k^n,\ \ \chi = \sum_{n=0}^{\infty}\chi_{(n)}k^n,\ \ \hat{p} = \sum_{n=1}^{\infty}p_{(n)}k^n \tag{56}$$

($_{(n)}$ are indices of summation constants) and $\omega = -k\chi$ from the kinematic boundary condition, gives

$$\omega = -3k + i\left(\frac{1}{3}P_{(1)} - \frac{6}{5}R_{(1)}\right)k^3. \tag{57}$$

Therefore at neutral stability

$$R_{(1)} = \frac{5}{18}P_{(1)}, \tag{58}$$

and

$$\tilde{k}_{cr} = \frac{6}{5}\left(\frac{27\,U^4}{\epsilon\ \beta^4}\frac{f_{\tilde{\alpha}}}{\left(1+f_{\tilde{\beta}}^2\right)\left(\frac{9}{\tilde{\beta}^2}-2+\frac{4f_{\tilde{\alpha}}f_{\tilde{\beta}}}{1+f_{\tilde{\beta}}^2}\right)}\right). \tag{59}$$

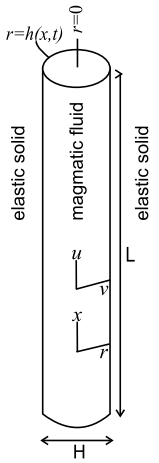

Figure 6: Geometry for our model with a cylindrical conduit. An incompressible, Newtonian fluid flows through a tube-like hole of length L and equilibrium diameter H in an elastic solid. Flow induced oscillations cause the tube radius (h) to vary in both x and time. Flow is two-dimensional with the along-tube velocity u much greater than the radial velocity v.

This result indicates that the across-gap-averaged model (53) is qualitatively correct but off by a factor of $\frac{6}{5}$.

7.4 Cylindrical conduit

Magma mostly rises through the Earth's brittle crust through fractures forming sheets of magma. Lava sometimes erupts from linear fissures, however, flow is usually localized by cooling, producing a cylindrical form at the top of the conduit. We assess the feasibility of flow through a cylindrical conduit generating tremor using long wave theory as done in section 7.3 for a crack.

We consider a fluid-filled tube of length L and diameter H in an elastic solid. The cylindrical coordinate system (x, r, θ) is set so that the x-axis is in the center of the tube and the solid-fluid interface is at $r = h(x, t)$. Flow is two-dimensional with velocity field $(u, v, 0)$ (Figure 6). We nondimensionalize as for the crack problem (4) with x and y replaced with z and r respectively. The non-dimensional governing equations for fluid flow are conservation of momentum,

$$\epsilon Re(u_t + uu_z + vu_r) = -P_z + \frac{1}{r}\frac{\partial}{\partial r}(ru_r), \quad P_r = 0, \tag{60}$$

and continuity,

$$u_z + \frac{1}{r}\frac{\partial}{\partial r}(rv) = 0. \tag{61}$$

We take the velocity of the fluid to be

$$U(r) = 2 - 2r^2, \tag{62}$$

so that the average velocity is one and the profile is parabolic. We define stream functions

$$u = \frac{1}{r}\frac{\partial}{\partial r}(r\chi) + U(r) \text{ and } v = -\chi_z, \tag{63}$$

where $\chi \propto e^{ikx+i\omega t}$. Using Bessel functions, matching of stresses in the Newtonian fluid and the elastic solid at their cylindrical interface gives

$$P = G[h(x,t) - 1] \left(\frac{2}{\epsilon} - \epsilon \, \ln(\epsilon \kappa_\alpha) \, \frac{\beta^2}{\alpha^2} \left(\frac{\alpha^2}{\beta^2} - 2 \right) (\kappa_\beta^2 + k^2) \right), \tag{64}$$

and thus

$$P \approx \frac{2G}{\epsilon}[h(x,t) - 1]. \tag{65}$$

Long wave expansion using the kinematic boundary condition (36), indicates that neutral stability for the cylindrical conduit occurs at

$$\frac{U^2}{\beta^2} \sim \frac{1}{\epsilon k}, \tag{66}$$

for small k, in contrast to

$$\frac{U^4}{\beta^4} \sim \epsilon k, \tag{67}$$

for the planar conduit. As discussed further below (section 9) for realistic parameter values, this result means that the cylindrical conduit is always much more stable to flow-induced oscillations than the planar conduit.

8 Non-linear stability analysis

Results from linear stability analysis are not necessarily a good indicator of the behaviour of non-linear systems. Our preliminary nonlinear analysis involves a periodic domain and the gap-averaged model (section 7.2) with the physically sensible simplifying assumption that $\omega << \alpha$ and $\omega << \beta$.

Given $h(x)$, we use a Fast Fourier Transform to compute fourier coefficients for the series

$$h - 1 = \sum_{n=-\infty}^{\infty} A_n e^{inx}. \tag{68}$$

Using these coefficients, the Fourier Transform solution for pressure at the wall for $\omega << \alpha$ and $\omega << \beta$ (33), and a Hilbert Transform, we have an expression for determining P_x,

$$P_x = i\hat{G} \sum_{n=-\infty}^{\infty} A_n \, n \mid n \mid e^{inx}, \tag{69}$$

where $\hat{G} = 2G \left(\frac{\alpha^2 - \beta^2}{\alpha^2} \right)$. With this P_x, inverted with a Inverse Fast Fourier Transform, the differential equations for momentum (44) and the kinematic boundary condition (46) are then solved by a MATLAB PDE solver (finite-difference method with standard time integrator). The end result is the evolution of h as a function of time and position along the crack (e.g., Figure 7). We varied both $\hat{G}$ and ϵRe by several orders of magnitude and set initial random or sinusoidal (k =1 to 6) perturbations in either h or in fluid flux. We found only simple, steady solutions; there was no complex behaviour such as multiplicity

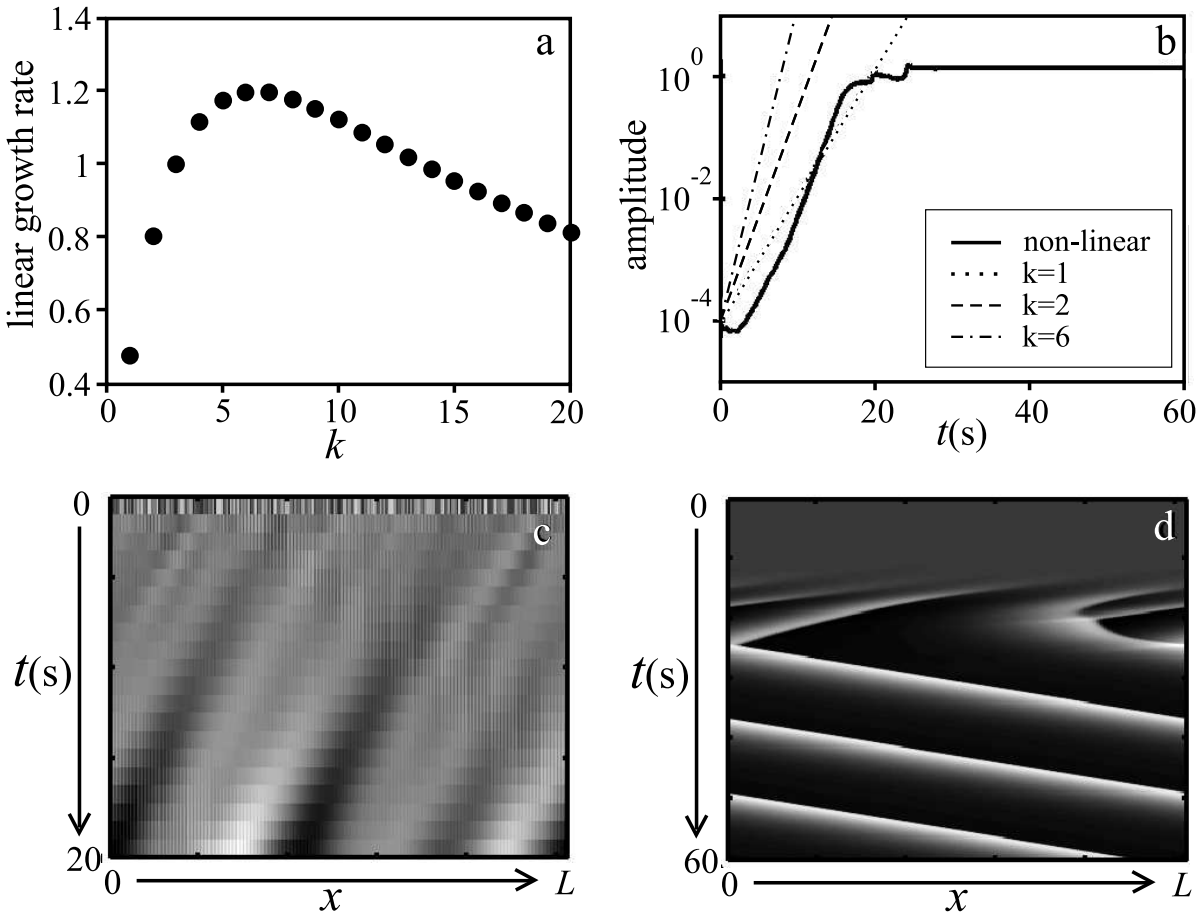

Figure 7: Results of a nonlinear simulation for $\epsilon Re = 2$ and $\hat{G} \equiv 2G\left(\frac{\alpha^2-\beta^2}{\alpha^2}\right) = 0.05$ beginning with random perturbations in h. For these parameters, the linear growth rate is greatest for $k \sim 6$ (a). (b) shows how the amplitude for the non-linear simulation changes with time (solid line). The broken lines illustrate growth rates for three k-values based on linear analysis. Subplots (c) and (d) show amplitude as a function of time and space (the horizontal axis is position along the crack of length L). The two subplots have different greyscales to maximize the range of tones but in both cases dark=high and light=low. A background speed of $2.5U$ was subtrated for more efficient computation and the apparent reversal in wave propagation in (d) is not real. (c) is the first 20 seconds of the simulation. Several waves form from the random perturbations. By 20 seconds it has coarsened to three waves. (d) is the first minute of the simulation. Note the sudden coarsening to two waves and then a single wave. The final wave has a very steep wave front (i.e., it is a roll wave).

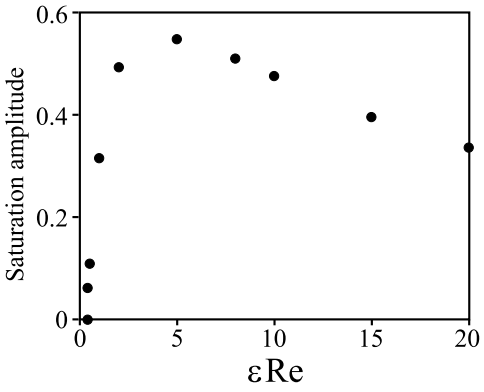

Figure 8: Plot of saturation amplitude versus ϵRe from non-linear analysis with a periodic domain and $\hat{G} \equiv 2G\left(\frac{\alpha^2-\beta^2}{\alpha^2}\right) = 1$. Amplitudes are normalized such that the equilibrium crack thickness is 2. The low saturation amplitude near the critical Re above which the system in unstable indicates a soft transition to instability (i.e., supercritical). This is unlike the familiar subcritical nature of turbulence where there is a sudden jump in behaviour above a critical Re.

or period-doubling. As shown in Figure 8, the transition from stable to unstable is "soft" with low-amplitude saturation near the critical Re.

No matter the initial conditions, when unstable, the waves coarsen to the longest possible wavelength ($k = 1$). Figure 8 shows an example where the linear growth rate, determined from the across-gap averaged model dispersion relation (48) for $\omega << \alpha$ and $\omega << \beta$,

$$\omega^2 + \left(\frac{12}{5}k + \frac{3}{i\epsilon Re}\right)\omega + \frac{6}{5}k^2 + \frac{9k}{i\epsilon Re} - 2G\left(\frac{\alpha^2-\beta^2}{\alpha^2}\right) = 0, \tag{70}$$

is greatest for $k \sim 6$. After some adjustment at the start, the non-linear growth rate is comparable to that for $k = 6$ and then decreases as the waves coarsen until finally the $k = 1$ wave becomes saturated. Coarsening indicates that the most unstable linear wave is not necessarily that observed and the character of tremor may be given by the lengthscale of cracks or crack constrictions. The $\hat{G}$ of 0.05 used in the simulation for Figure 7 is much lower than expected for the volcanic system but was chosen to demonstrate coarsening. In the real volcanic system, the highest growth rate is probably $k \sim 1$ or $k \sim 2$ and the coarsening behaviour (transition to lower k until $k = 1$) is less evident.

9 Back to volcanoes

Our linear stability analysis suggests that for flow through a crack in an elastic solid, flow-induced oscillations are possible at arbitrarily low, non-zero Reynolds numbers. Furthermore, the stability of the system depends on the crack aspect ratio, fluid speed and elastic wave speeds. However, to this point we have not considered the physical parameters relevant to volcanic tremor. From (53), the range of wavenumbers and Reynolds numbers for which the system is unstable expands (to lower k and Re) if the crack thickness to length ratio or the shear wave speed in the rock are decreased. To assess the feasibility of our model

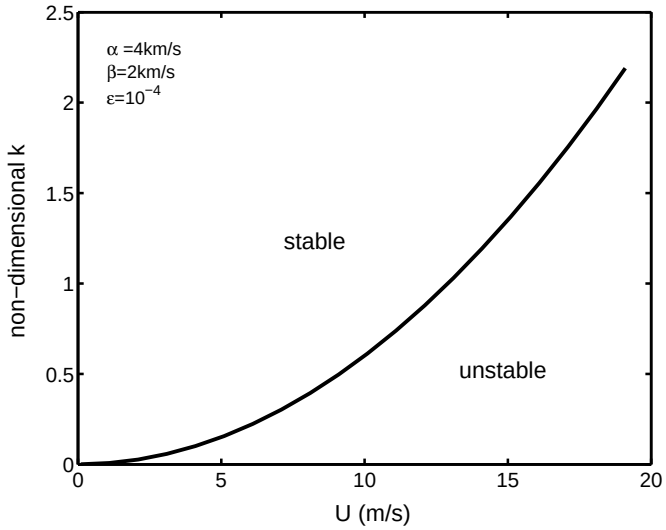

Figure 9: The curve on this plot of non-dimensional wavenumber versus average fluid velocity represents neutral stability for flow through a crack with aspect ratio $\epsilon = 10^{-4}$ in a solid with elastic wavespeeds $\alpha = 4$ km/s and $\beta = 2$ km/s. The plot is based on results of the averaged velocity model (53) with the slight correction from long wave theory $\left(\frac{6}{5}\right)$.

for generating volcanic tremor we consider $\epsilon = 10^{-4}$ and $\beta = 2$ km/s, which are at the low end of physically possible parameters. We require that the nondimensional wave number, $\tilde{k}$, be at least 1 which corresponds to a wavelength equal to the length of the crack (4). Figure 9 shows that even using these relatively low ϵ and β values, average fluid velocities of order 10 m/s or greater are needed to induce oscillations. Thus the feasibility of the model reduces to the feasibility of fluids flowing at speeds of order 10 m/s through cracks beneath volcanoes. Stability does not depend directly on viscosity but the more viscous the fluid, the greater the pressure gradient needed to drive flow at a given velocity through a crack with a given aperture. The required conditions of high flow speeds through thin cracks are most easily achieved for low viscosity fluids such as convecting groundwater or vapors and supercritical fluids exsolved from magma. There is potential for tremor triggered by such fluids to be common because aqueous fluids are present at all volcanoes and eruptions of magma are typically preceded by increased gas emissions.

To what depths are aqueous fluids present? There is growing evidence from volcanic gas emissions as well as the chemistry of crystals and pockets of melt trapped inside crystals, that magmas in storage regions kilometers below volcanoes are often saturated in volatiles (mixtures of H_2O, CO_2, etc.) [12]. For example, melt inclusions in quartz crystals indicate that the magma that became the Bishop Tuff (Long Valley, California) exsolved enough volatiles to comprise 30% by volume of the magma prior to rapid ascent and eruption [13]. Because of the low viscosity and density of the volatile phase, and the increased fluid pressure caused by its formation, a portion of this supercritical aqueous fluid likely rose through cracks in rock above the magma. Further evidence for aqueous fluid flow at several kilometers depth is preserved in porphyry deposits. The porphyry copper-gold mine in Butte Montana for instance, contains countless veins formed by aqueous fluids flowing

through rock fractures that were once about 7 km beneath a volcano [14].

Typically one does not expect there to be a free volatile phase below 10 km depth because the solubility of volatiles in silicate melts increases with increasing pressure. However, saturation at great depth is possible if there is sufficient CO_2 in the melt. To take an extreme (and exceedingly rare) example, kimberlite magmas, the most common source of diamonds, are thought to contain about 30% CO_2 by **weight** and saturate in volatiles at about 150 km depth. The deepest reported tremor originated about 40 km below Kilauea Volcano, Hawaii [15] in the 1970's. Recent data on gas emissions from the summit of Kilauea [16] show a surprisingly high CO_2 emission rate ($\approx 8.5 \times 10^6$ kg/day), which, in conjunction with information on the chemistry and supply rate of the magma, indicates that the basalt contained about 0.7 % CO_2 by weight and saturated in volatiles at about 0.95 GPa. For inferred crust and upper mantle densities [17], this means that volatile exsolution from the magma to form a low viscosity, low density fluid, could occur about 30 km under Kilauea [16]. Although not as deep as the deepest tremor reported by Aki and Koyanagi, the data of Gerlach et al. open the possibility that a volatile phase played a role in generating the deep sustained vibrations below Kilauea. It is possible for there to be a free volatile phase at greater depths than 30 km without invoking greater bulk CO_2 contents in the basalt. Crystallization of basalt concentrates CO_2 in the melt because the crystals contain negligible CO_2. Thus, substantial crystallization of basalt stalled at 40 km depth could leave a residual melt that is saturated in CO_2. Pressure increase from the exsolution of a low-density fluid could cause fractures in the overlying rock through which the CO_2-rich fluid escapes. In fact sudden onsets to the deep tremor at Kilauea reported by [15] are what allowed Aki and Koyanagi to locate the source depths. We conclude that flow of aqueous or CO_2-rich fluids is a plausible source mechanism for volcanic tremor in the upper several km of crust where most tremor is generated as well as deep tremor for magmas with high CO_2 contents.

It is also possible that magma transport could generate tremor in the upper crust during explosive eruptions and fire-fountaining as exit velocities for these eruption styles can reach hundreds of m/s and 50 m/s, respectfully [18, 19]. However, the viscosity of magma (10 to 10^{12} Pa s) makes sustained velocities of 10 m/s unreasonable for subsurface magma flow that is not coincident with, or immediately preceding, eruption of magma at the surface. Very thick dikes reduce the resistance to flow and thus may allow large magma velocities but our scaling of the problem (4), combined with the frequencies of volcanic tremor, limit the size of the crack. The characteristic time scale is $t = \frac{L}{U}$, and as the period of tremor is typically seconds, the length of the crack (in m) cannot be more than an order of magnitude greater than the average fluid velocity (in m/s). To keep the minimum fluid velocity required for flow-induced oscillations down to $\mathcal{O}(10$ m/s), we used $\epsilon = 10^{-4}$. With our time-scale constraints, the crack could be as long as $\mathcal{O}(100$ m) which gives a crack thickness of only $\mathcal{O}(1$ cm). For laminar flow of basalt with $\mu = 100$ Pa s, this corresponds to a pressure gradient of $\mathcal{O}(10^8$ Pa/m) and decompression rate of $\mathcal{O}(10^9$ Pa/s), values which are probably only reached by rapid bubble expansion and fragmentation at shallow levels during explosive eruptions. Therefore, linear stability analysis suggests that magma transport is unlikely to generate flow induced oscillations except at shallow levels (perhaps top 2 km) during explosive or fountaining eruptions. If a low viscosity fluid is required for deep tremor, this could explain the general lack of long period seismicity in recharge zones

beneath intermediate and silicic volcanoes where there is magma movement but the magma is not saturated in volatiles.

Our analysis indicates that some fluids, conduit geometries and eruption styles are more likely to cause tremor by flow-induced oscillations than others. In particular, we found that planar rather than tube-like fluid conduits, small thickness to length ratios of conduits, and high fluid speeds are factors that tend to generate flow-induced tremor. Except for shallow seismicity during explosive or fountaining activity, for realistic pressure gradients, maintaining sufficient fluid speeds (>10 m/s) to induce oscillations requires sustained flow of low viscosity aqueous or carbonaceous fluid rather than magma. These conclusions from stability analysis are consistent with observations by McNutt [3] in a study of tremor from 50 eruptions at 31 volcanoes comparing tremor characteristics and corresponding eruption parameters. McNutt lists four trends in the data:
"1) large eruptions produce stronger tremor than small ones;
2) fissure eruptions produce stronger tremor than circular vents for the same fountain height;
3) eruptions with higher gas content produce stronger tremor than those with low gas content at the same volcano; and
4) phreatic eruptions [*eruptions that eject broken rock and vapor but no magma*] produce stronger tremor than magmatic eruptions [*eruptions that do eject magma*] for the same VEI [*Volcanic Explosivity Index, a measure of the magnitude and intensity of an eruption*]."
Therefore, flow-induced oscillations are a plausible source mechanism for volcanic tremor that is consistent with observations from volcanoes.

10 Future work

There are several possible avenues for future research. These include fluid compressibility, non-linear analysis with a non-periodic domain and application of results to other systems. Perhaps the simplest and most obvious is to add fluid compressibility. We concluded that flow-induced tremor is most readily generated by flow of vapors and other aqueous fluids through cracks. The compressibility of these fluids will be significant at pressures in the first few kilometers below volcanoes and thus we will incorporate compressibility in the across-gap averaged model.

Further non-linear analysis is required. Our preliminary model involving a crack with a periodic domain may not be adequate as it does not produce period doubling, a non-linear phenomenon observed at several volcanoes. The difficulty in treating the fluid conduit as a slot with a non-periodic domain is setting the boundary conditions.

In addition to volcanic tremor, the generation of oscillations by flow past a deformable material has applications in diverse fields such as physiology [11] and drag reduction in gel-lined tubes and other surfaces [20]. It would be interesting to examine our results for conditions relevant to these applications (e.g., much lower elastic velocities).

11 Acknowledgements

Thanks so much to Neil Balmforth for his help and patience supervising me this summer. I definitely needed more help than a typical fellow but I also learned much more than a

typical fellow. Thanks also to my fellow fellows and other inhabitants of The Palace for a tasty summer.

References

[1] B. R. Julian, "Volcanic tremor: Nonlinear excitation by fluid flow," J. Geophys. Res. **99**, 11859 (1994).

[2] K. I. Konstantinou and V. Schlindwein, "Nature, wavefield properties and source mechanism of volcanic tremor: a review," J. Volc. Geotherm. Res. **119**, 161 (2002).

[3] S. R. McNutt, "Volcanic tremor and its use in estimating eruption parameters," Eos Trans. Amer. Geophys. Un., Fall Meeting Suppl. **83**, F1500 (2002).

[4] B. R. Julian, "Period doubling and other nonlinear phenomena in volcanic earthquakes and tremor," J. Volc. Geotherm. Res. **101**, 19 (2000).

[5] B. A. Chouet, "Dynamics of a fluid-driven crack in three dimensions by the finite difference method," J. Geophys. Res. **91**, 967 (1986).

[6] B. A. Chouet, "Resonance of a fluid-driven crack: radiation properties and implications for the source of long-period events and harmonic tremor," J. Geophys. Res. **93**, 4375 (1988).

[7] B. A. Chouet, "A seismic model for the souce of long-period events and harmonic tremor", in: P. Gasparini, R. Scaarppa, and K. Aki (eds.), *Volcanic Seismology*, (IAVCEI, 1992).

[8] F. G. Cruz and B. A. Chouet, "Long-period events, the most characteristic seismicity accompanying the emplacement and extrusion of a lava dome in Galeras Volcano, Colombia, in 1991," J. Volc. Geotherm. Res. **77**, 121 (1997).

[9] B. A. Chouet, R. A. Page, C. D. Stephens, J. C. Lahr, and J. A. Power, "Precursory swarms of long-period events at Redoubt Volcano (1989-1990), Alaska; their origin and use as a forecasting tool," J. Volc. Geotherm. Res. **62**, 95 (1994).

[10] M. M. Morrissey and B. A. Chouet, "Trends in long-period seismicity related to magmatic fluid compositions," J. Volc. Geotherm. Res. **108**, 265 (2001).

[11] T. J. Pedley, *Fluid Mechanics of Large Blood Vessels* (Cambridge University Press, Cambridge, 1980).

[12] P. J. Wallace and A. T. Anderson, *Volatiles in magma*, in: H. Sigurdsson, B. Houghton, S. R. McNutt, H. Rymer and J. Stix (eds.), *Encyclopedia of Volcanology,* (Elsevier Science & Technology Books, 1999).

[13] P. J. Wallace, A. T. Anderson, and A. M. Davis, "Gradients in H_2O, CO_2, and exsolved gas in a large-volume silicic magma system: Interpreting the record preserved in melt inclusions from the Bishop Tuff," J. Geophys. Res. **104**, 20097 (1999).

[14] B. Rusk, M. H. Reed, J. H. Dilles, L. Klemm, and C. A. Heinrich, "Fluid inclusion evidence for magmatic fluid evolution in the porphyry copper deposit; Butte, Montana," Geol. Soc. Am., Cord. Sect., 98th annual meeting, Abstracts with Programs **34**, 16 (2002).

[15] K. Aki and R. Koyanagi, "Deep volcanic tremor and magma ascent mechanism under Kilauea, Hawaii," J. Geophys. Res. **86**, 7095 (1981).

[16] T. M. Gerlach, K. A. McGee, T. Elias, A. J. Sutton, and M. P. Doukas, "Carbon dioxide emission rate of Kilauea Volcano: Implications for primary magma and the summit reservoir," J. Geophys. Res. **107**, ECV3 1 (2002).

[17] M. P. Ryan, "Neutral boyancy and the mechanical evolution of magmatic systems", in: B. O. Mysen (ed.) *Magmatic processes: Physiochemical principles*, Spec. Publ. Geochem. Soc. **1**, 259 (1987).

[18] F. Dobran, *Volcanic Processes: Mechanisms in Material Transport* (Kluwer Academic Publishers Group, 2001).

[19] M. T. Mangan and K. V. Cashman, "The structure of basaltic scoria and reticulite and inferences for vesiculation, foam formation, and fragmentation in lava fountains," J. Volc. Geotherm. Res. **73**, 1 (1996).

[20] V. Shankar and V. Kumaran, "Stability of wall modes in fluid flow past a flexible surface," Phys. Fluids **14**, 2324 (2002).